G. Löwisch, H. Bomas,* and P. Mayr**

Fatigue Crack Initiation and Propagation in Ductile Steels under Multiaxial Loading

REFERENCE Löwisch, G., Bomas, H., and Mayr, P., **Fatigue crack initiation and propagation in ductile steels under multiaxial loading**, *Multiaxial and Fatigue Design*, ESIS 21 (Edited by A. Pineau, G. Cailletaud, and T. C. Lindley) 1996, Mechanical Engineering Publications, London, pp. 243–259.

ABSTRACT Fatigue behaviour of thin-walled tubular specimens subjected to tension and torsion loading as well as in-phase and out-of-phase combined tension–torsion loading was investigated using the ferritic steel Ck15 and the austenitic steel X2 CrNiMnMoNNb 21 16 5 3. In addition to lifetime and deformation behaviour the development of microcracks was observed. Cracks occur in the plane of maximum shear-stress amplitude except under out-of-phase loading of the stainless steel. The variations of the used equivalent stress criterion necessary to explain the lifetime of the specimens may be explained by the crack growth behaviour of microcracks and their interaction with barriers.

Notation

a	half-crack length
C	material constant
k	weighting factor for normal stress (Findley criterion)
m	weighting factor for shear stress amplitude (modified stress criteron)
n	multiplier for the Findley criterion
N	number of cycles
N_f	number of cycles to failure
δ	phase angle
$\varepsilon(t)$	actual normal strain
ε_p	plastic normal strain
$\varepsilon_{pa\ EQ\ vM}$	von Mises plastic equivalent strain amplitude
$\gamma(t)$	actual shear strain
γ_p	plastic shear strain
λ	loading ratio: τ_a/σ_a
ν	Poissons ratio
ϕ	crack angle
$\sigma(t)$	actual normal stress

*Stiftung Institut für Werkstofftechnik, Bremen, Germany.

σ_a	normal stress loading amplitude
$\sigma_{tension}$	stress amplitude for pure tension loading
$\sigma_{a\,EQ\,T}$	Tresca equivalent stress amplitude
$\sigma_{a\,EQ\,vM}$	von Mises equivalent stress amplitude
$\sigma_{a\,EQ\,mod}$	modified equivalent stress amplitude
$\sigma_{a\,EQ\,F}$	Findley equivalent stress amplitude
$\tau(t)$	actual shear stress
τ_a	shear stress loading amplitude
$\tau_{torsion}$	shear stress amplitude for pure torsion loading
τ_{max}	shear stress amplitude in a critical plane

1 Introduction

A large number of studies has been devoted to investigating the extraordinary out-of-phase hardening effect in FCC materials like AISI 316, while ferritic steels have not been investigated so thoroughly. Especially the microscopic events during complex loading, leading to alterations in the lifetime of the specimen, have not been investigated yet. The aim of this investigation is to analyse microscopic mechanisms like crack initiation and formation of dislocation structures and to relate them to the measured deformation behaviour and the lifetime of the specimen. Therefore a ferritic steel, which is known to produce a dislocation cell structure under cyclic loading and a high-alloyed austenitic steel with a planar slip character were selected.

2 Equivalent Stress Hypotheses

The most used equivalent stress criteria for ductile steels in the low- and medium-cycle fatigue areas are the von Mises ($\sigma_{a\,EQ\,vM}$)) and the Tresca ($\sigma_{a\,EQ\,T}$) criterion. For combined tension and torsion in-phase loading these criteria are described by the formula

$$\sigma_{a\,EQ} = \sqrt{\sigma_a^2 + m^2\tau_a^2} \tag{1}$$

with σ_a, τ_a = normal stress, shear stress loading amplitude; $m^2 = 4$ for Tresca criterion and $m^2 = 3$ for von Mises criterion, respectively.

One can consider the value m as a factor describing how harmful a torsional loading is compared to tension loading

$$m = \sigma_{tension}(N_f)/\tau_{torsion}(N_f) \tag{2}$$

with $\sigma_{tension}$, $\tau_{torsion}$ = amplitudes for pure tension and pure torsion loading leading to the same lifetime, N_f = constant.

If we use this value of m, obtained from experimental data, instead of the von Mises value $m = \sqrt{3}$ or the Tresca value $m = 2$, we call this modification of the equivalent stress $\sigma_{EQ\,mod}$.

For out-of-phase loading another modification is necessary to take account of rotating principal axes. Usually the maximum value of the equivalent stress during one cycle is applied.

$$\sigma_{a\,EQ\,mod} = \max\sqrt{\sigma(t)^2 + m^2\tau(t)^2} \tag{3}$$

In a similar way one can calculate an equivalent plastic strain amplitude using the measured strain response and calculating the plastic part using the following equations

$$\varepsilon_p = \varepsilon - \sigma/E \text{ and } \gamma_p = \gamma - 2\,\tau(1+\nu)/E \tag{4}$$

with $E = 204\,000$ N/mm^2 (ferritic steel) and 190 200 N/mm^2 (austenitic stainless steel) and $\nu = 0.5$

$$\varepsilon_{a\,EQ\,mod} = \max\sqrt{\varepsilon_p^2 + m^2\gamma_p^2} \tag{5}$$

For the Tresca criterion one can interpret this procedure as a critical plane approach, seeking the plane loaded with the maximum shear stress amplitude. Another critical plane approach, considering also the normal stress perpendicular to the plane of maximum shear stress amplitude is the equivalent stress criterion proposed by Findley (1)

$$C = \tau_{max} + k\sigma_n \tag{6}$$

with τ_{max} = shear stress amplitude in the critical plane; σ_n = normal stress amplitude on the plane; k = material constant, calculated from the Wöhler curve for tension and torsion loading.

In order to obtain a comparable value, C may be replaced by an equivalent stress amplitude comparable to the uniaxial fatigue data

$$\sigma_{a\,EQF} = n(\tau_{max} + k\sigma_n) \tag{7}$$

where n is a function of k, being 2 for $k = 0$.

3 Material, Specimens, and Loading Conditions

The materials used were a low carbon steel in a normalized condition and an austenitic steel. The chemical composition and the conventional mechanical properties are listed in Tables 1 and 2. The average grain size was 23 μm and 18 μm, respectively. Pure tension–compression, pure torsion and combined tension and torsion tests, either in-phase or 90° out-of-phase with a loading ratio $\lambda = \tau_a/\sigma_a = 0.5$ were carried out.

Table 1 Chemical composition of the materials used (wt.%)

Ferritic steel; Ck 15

C	Si	Mn	P	S
0.17	0.22	0.50	0.017	0.008

Austenitic stainless steel; X2 CrNiMnMoNNb 21 16 5 3

C	Si	Mn	P	S	Cr	Mo	Ni	Nb	N	V	Co	Ti
0.022	0.44	4.45	0.022	0.009	19.7	3.24	15.6	0.11	0.42	0.07	0.16	0.01

Table 2 Properties of the materials used

	Ferritic Steel Ck 15	*Austenitic stainless steel* X2 CrNiMnMoNNb 21 16 5 3
Initial condition	normalized	annealed and quenched
Yield strength $R_{eH}/R_{p0,2}$	313 N/mm²	458 N/mm²
Tensile strength R_m	474 N/mm²	817 N/mm²
Crack elongation A_5	37%	46 %
Reduction of area Z	64%	74%

The tests were conducted on servohydraulic test equipment for axial and torsional loads under normal and shear stress control. In order to produce a homogeneous stress distribution, thin-walled tubular specimens with 18 mm inside diameter, 21 mm external diameter and a gauge length of 30 mm were used. The outer surface was mechanically polished (ferritic steel) or electropolished (austenitic steel), respectively. The interior surface was honed. The ferritic specimens, which were used only for lifetime and deformation behaviour investigation had a precisely turned surface to avoid work.

4 Deformation Behaviour

The elastoplastic behaviour of low carbon steels under uniaxial loading as described, for example, by Pilo (**2**) was also confirmed under torsional and combined in- and out-of-phase loading of the ferritic steel. During the first cycles of the loading the ferritic material behaves elastically. After a number of cycles a rapid softening effect occurs followed by a region of mainly hardening behaviour. The rapid softening stage is explained in literature by the unlocking of fixed dislocations from interstitial solute atoms.

The cyclic stress–strain curve of the material is plotted in Fig. 1, using the value of the plastic strain amplitude at $N_f/2$. The von Mises equivalent stress strain criterion leads to the same stress–strain curve for the uniaxial, the torsional, and the in-phase loading, respectively. Under out-of-phase loading a small extra hardening effect is observed. An out-of-phase hardening in the order of magnitude as found for austenitic steels does not occur. An investigation of

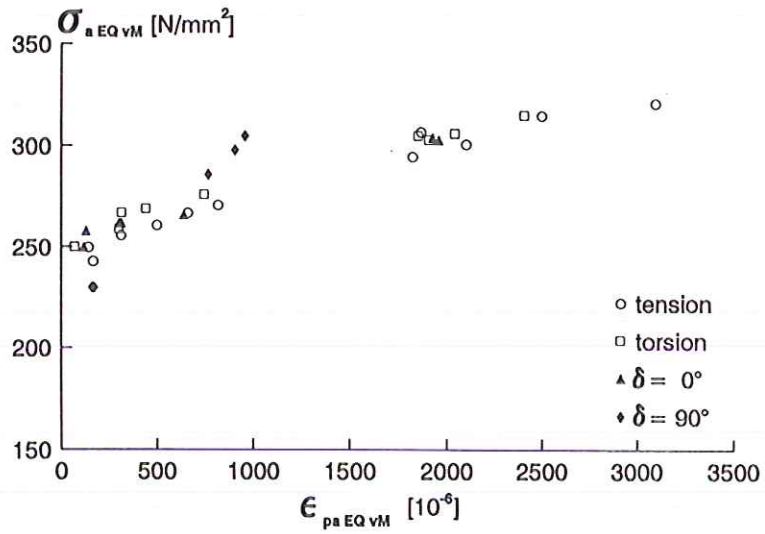

Fig 1 Ferritic steel: cyclic stress–strain curve for different loadings.

the dislocation structure by TEM shows a dislocation cell structure for every loading condition. Using a Weibull distribution to describe the magnitude of the cells we found a 30 percent smaller cell width after the out-of-phase loading than after the other loading conditions (Fig. 2).

The austenitic steel shows a cyclic softening behaviour without reaching a saturation. Therefore the cyclic stress–strain curve plotted in Fig. 3 is determined with a big scatter in the plastic strain amplitude at $N_f/2$. The unusual behaviour of the austenitic stainless steel may be explained by the kind of dislocation substructure. Although a high plastic strain amplitude is obtained, the dislocation density is low. Therefore the dislocation movement is not hampered.

Against the experience obtained from investigations with stainless steel like AISI 316 (3) we observed no extra hardening effect associated with out-of-phase loading. This behaviour can also be explained by the results of TEM investigations (Fig. 4). Plastic deformation means dislocation movement in several slip planes in the case of out-of-phase loading, but in only one slip plane for proportional loading. For out-of-phase loading the dislocation initiation is easier, due to the increased number of slip systems which leads to an extra softening. On the other hand, the dislocation interaction due to the increased dislocation density and due to crossing slip planes leads also to an extra hardening. Both effects cancel each other at the investigated loading amplitudes.

5 Cracks

The arising plastic deformations during fatigue loading lead to crack initiation

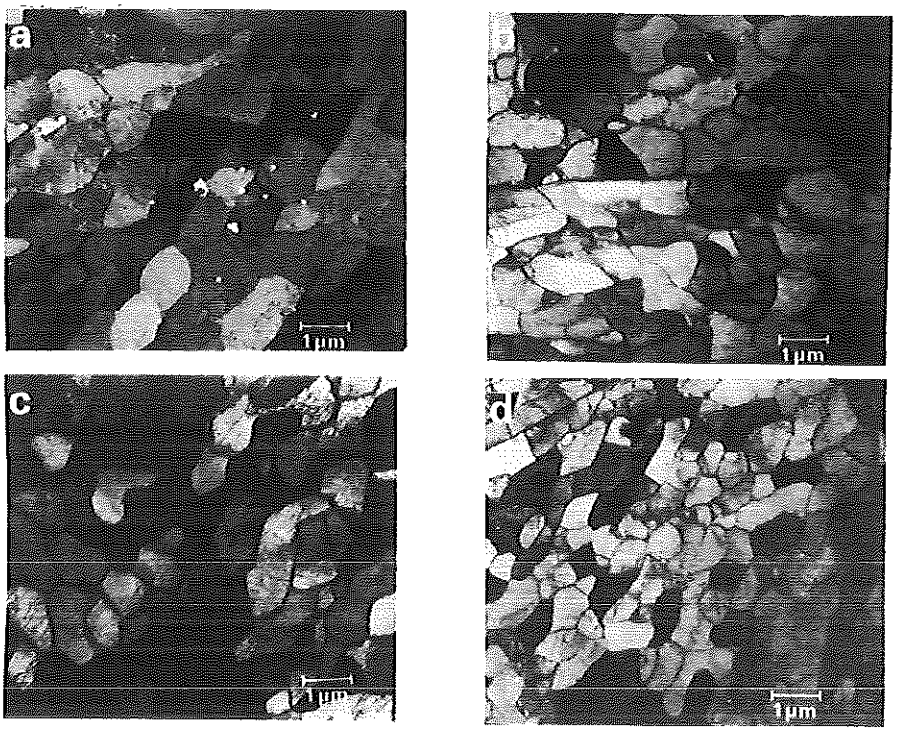

Fig 2 Dislocation structure in the ferritic steel after loading: (a) tensile loading $\sigma_a = 300$ N/mm^2, average area of the dislocation cells $A_c = 1{,}26$ μm^2; (b) torsional loading $\tau_a = 175$ N/mm^2, $A_c = 1{,}31$ μm^2; (c) combined in-phase loading $\sigma_a = 230$ N/mm^2, $\tau_a = 150$ N/mm^2, $A_c = 1{,}36$ μm^2; (d) combined out-of-phase loading $\sigma_a = 300$ N/mm^2, $\tau_a = 150$ N/mm^2, $A_c = 1{,}06$ μm^2.

in the material after a certain number of cycles. The first cracks can occur at a very early stage of the fatigue lifetime. For that reason the mechanisms of crack initiation and crack propagation are important for the lifetime of a specimen. In order to investigate these mechanisms an area of 1×4.8 mm^2 was observed by a light microscope with a magnification of 130:1 after various numbers of cycles. This was applied on six specimens for each loading mode. In order to have a clear crack identification only cracks with a length of more than 55 μm were evaluated. The direction of a crack was defined as the favoured growth direction which was observed after failure. The crack direction was determined by the angle between the specimen axis and the perpendicular to the favoured growth direction. The length of the crack was defined as the projection of the crack on the growth direction (Fig. 5).

Crack initiation in the ferritic steel takes place at the surface and depends strongly on the applied stress amplitude. At high amplitudes the cracks initiate during the first half of the lifetime. During the second half mainly crack growth and coalescence occur whereas the crack initiation rate decreases. Hardly any difference is observed between the crack densities for the different loading

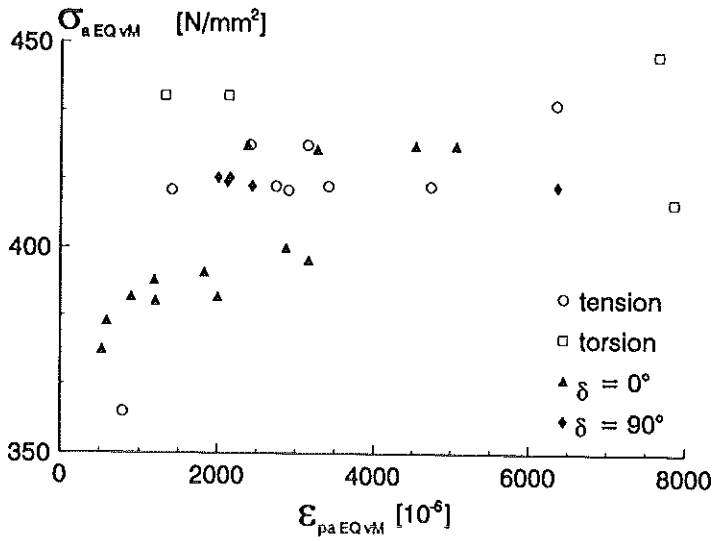

Fig 3 Austenitic stainless steel: cyclic stress–strain curve for different loadings.

conditions as shown in Fig. 6. At low amplitudes the crack density increases linearly right from the beginning. Only a few cracks grow together which can be attributed to the lower crack density. The specimens subjected to torsional and the combined in-phase loadings possess a higher crack density than the other specimens (Fig. 6).

A similar development of cracks was observed for the austenitic steel at high amplitudes (Fig. 7). The crack density increases linearly right from the beginning, leading to a higher crack density for torsional and in-phase loadings, compared to the other ones.

Generally, with increasing number of cycles the crack length spectrum enlarges and moves in the direction of longer cracks. The crack length obey in sections a Weibull distribution (4). Deviations are found at longer crack-lengths caused by the coalescence of cracks.

Many of the observed cracks stopped growth during cycling. Crack growth diagrams were established for those cracks, which showed high growing rates. Figure 8 shows one typical example of these diagrams. For short cracks the growth rate is observed to decrease with increasing crack length. It represents the behaviour of shear stress controlled microcracks (5, 6) which possess shorter crack lengths than the critical length at which the macroscopic crack propagation starts. This is confirmed by the long crack curve of a similar steel with equal mechanical properties (7) shown in Fig. 8. After decreasing, a subsequent increasing of the crack growth rate was observed for the austenitic steel. The crack length where the increasing occurs is different for all cracks.

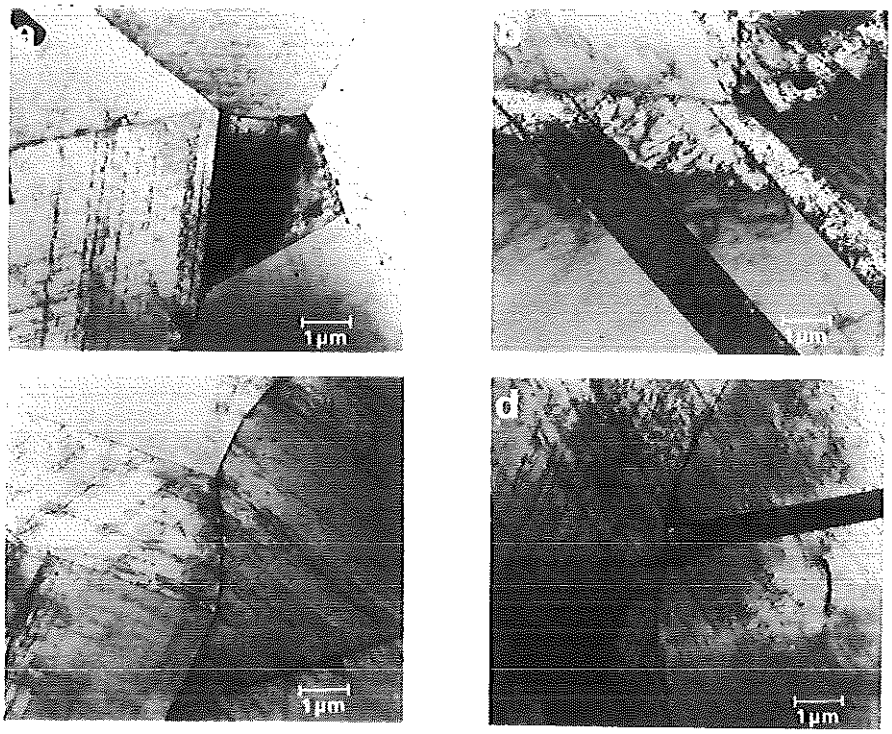

Fig 4 Dislocation structure in the austenitic steel after loading; (a) tensile loading $\sigma_a = 410$ N/mm^2; (b) torsional loading $\tau_a = 255$ N/mm^2; (c) combined in-phase loading $\sigma_a = 410$ N/mm^2, $\tau_a = 205$ N/mm^2.

From a shear stress controlled crack growth it is expected that cracks occur in certain planes. Therefore in Figs 9 and 10 the orientation of the microcracks is plotted in histograms. Additionally the frequency of the angles of intersection lines between the specimen surface and the planes with maximum shear stress amplitude is plotted as a continuous line. The crack initiation is supposed to occur through irreversible slip processes along activated slip planes. To explain the deviation between the theoretical and actual distribution of crack directions it has to be considered that due to crystallographic reasons only a limited number of favourably orientated slip planes exists. For that reason the crystallographic plane of the activated slip system can considerably deviate from the calculated plane containing the maximum shear stress amplitude. Nevertheless a good coincidence was observed between the calculated and the measured crack directions except for the out-of-phase loading of the austenitic steel. Here a better coincidence is found by taking into account the normal stress perpendicular to the critical plane as proposed by Findley. In Fig. 11 the expected histogram of crack angles using the criterion

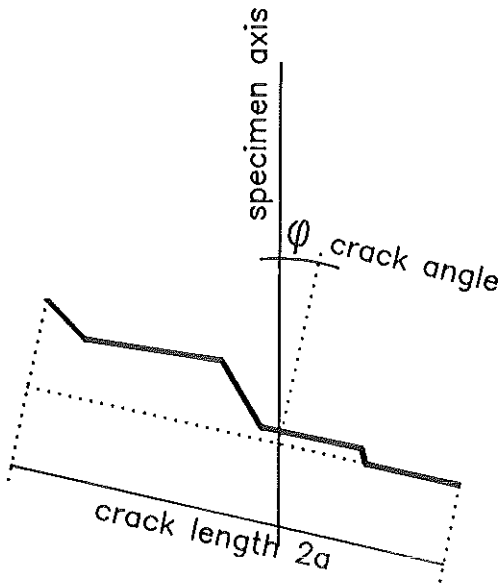

Fig 5 Definition of crack angle and crack length.

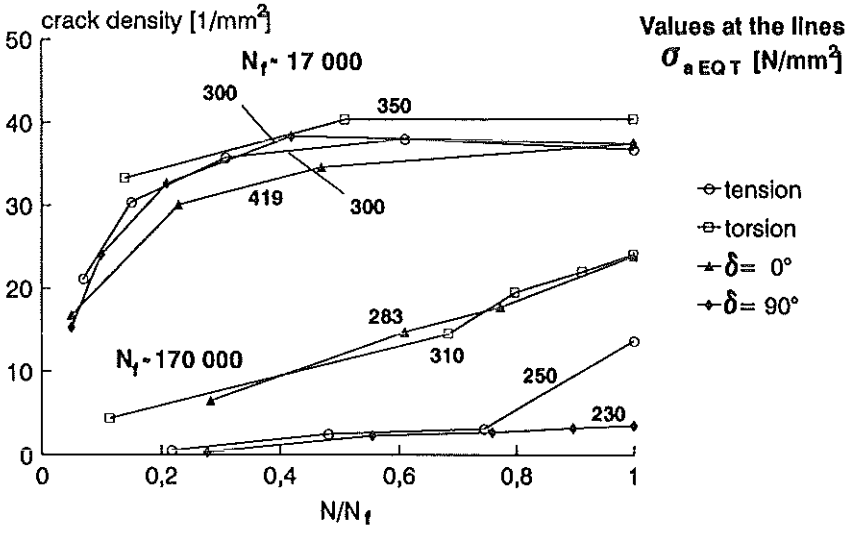

Fig 6 Ferritic steel: crack density during lifetime.

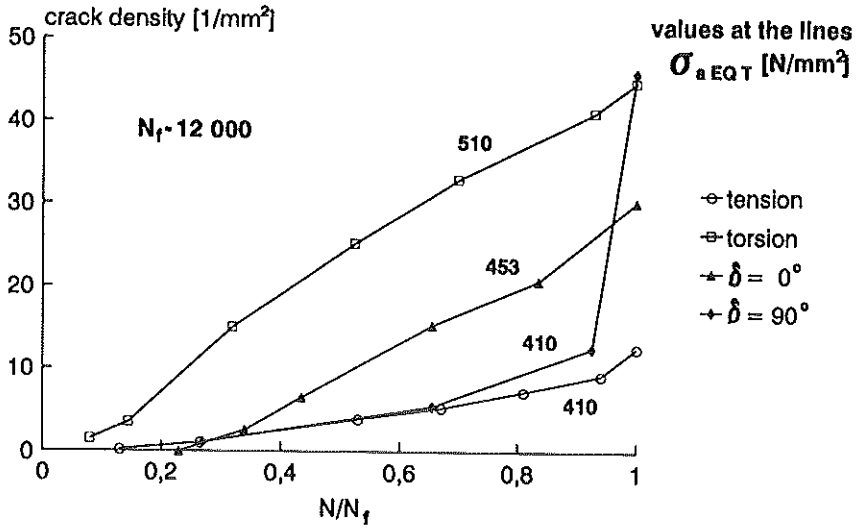

Fig 7 Austenitic stainless steel: crack density during lifetime.

$$C = \tau_{max} + k\sigma_n \tag{8}$$

with $\bar{k} = 0.0845$ and 0.126 are plotted for both materials. This value k is half of the value calculated from the tension and torsion data, which were found to

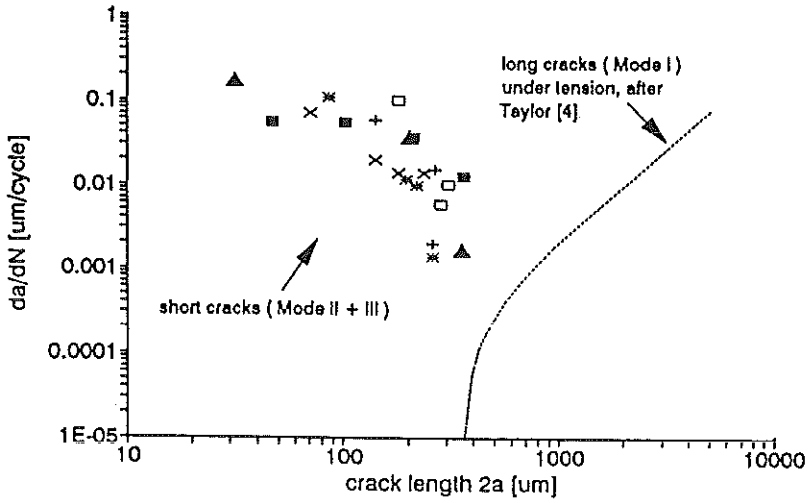

Fig 8 Crack growth of selected linking cracks under tension loading with $\sigma_a = 300$ N/mm². Every symbol represents one crack.

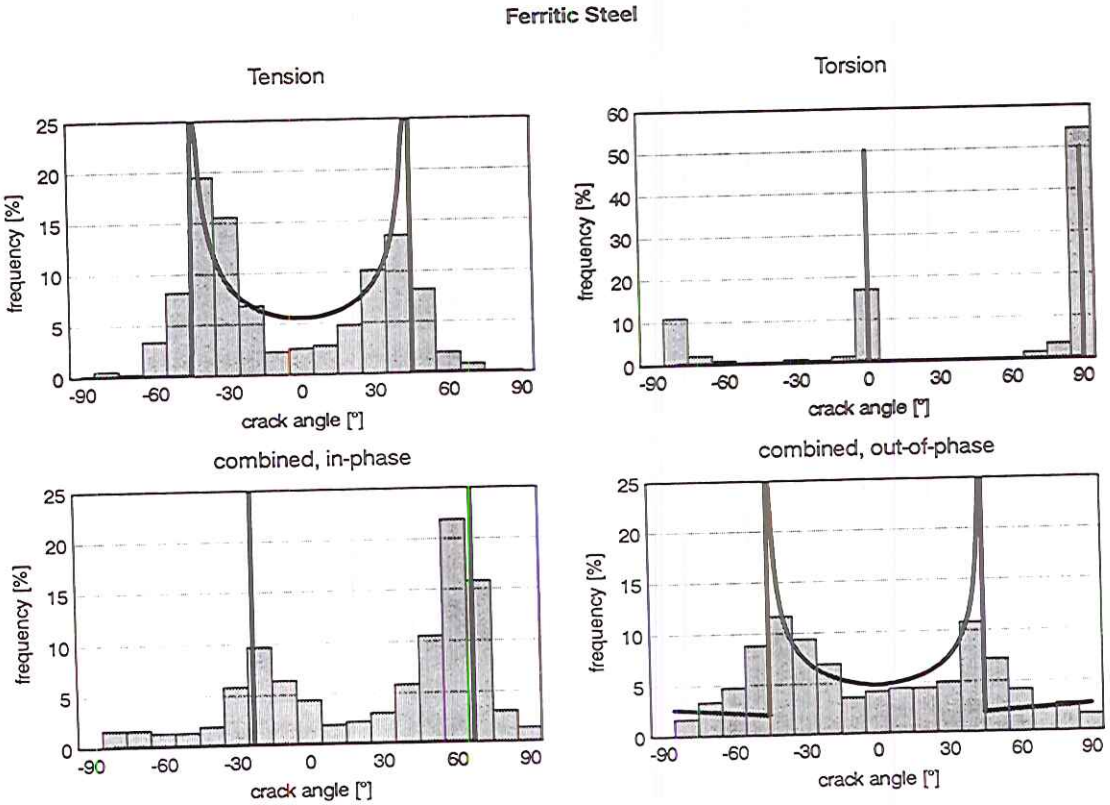

Fig 9 Crack orientation frequencies for the ferritic steel ($N_f \approx 17\,000$). Blocks: measured frequencies; continuous line: frequencies of planes loaded with maximum shear stress amplitude.

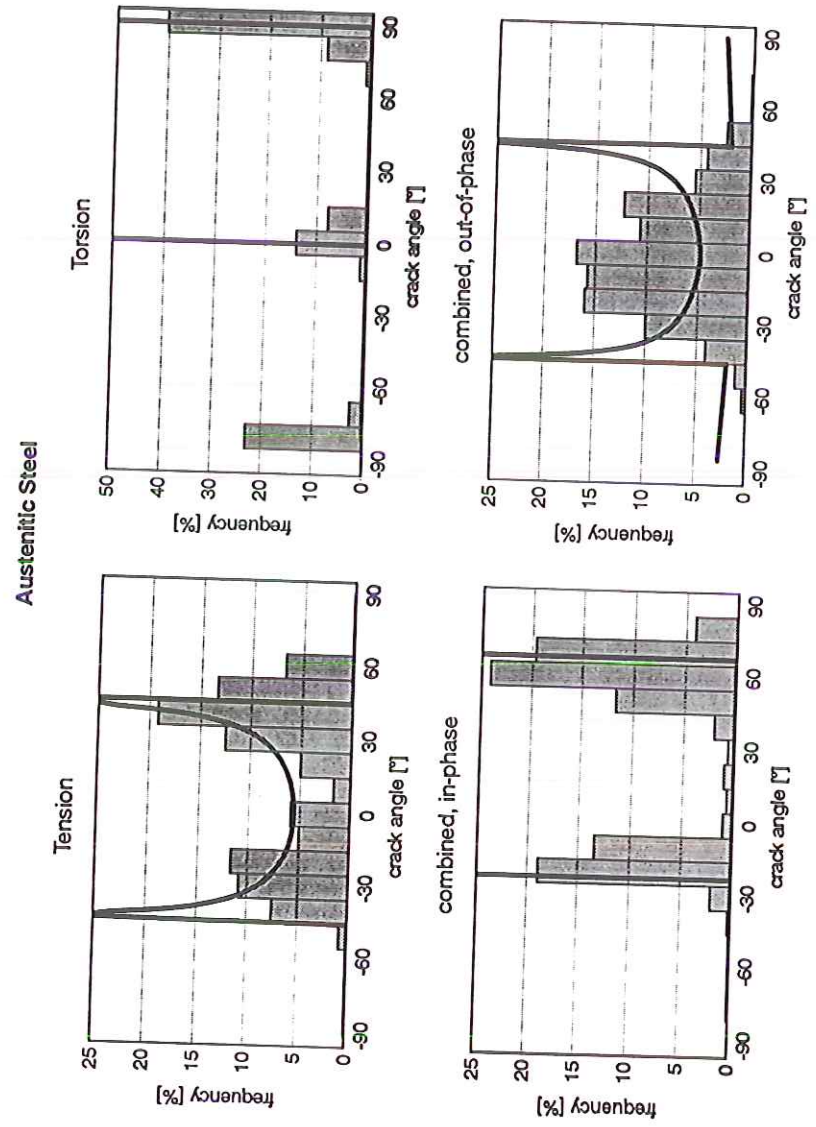

Fig 10 Crack orientation frequencies for austenitic stainless steel ($N_f \approx 12\,000$). Blocks: measured frequencies; continuous line: frequencies of planes loaded with maximum shear stress amplitude.

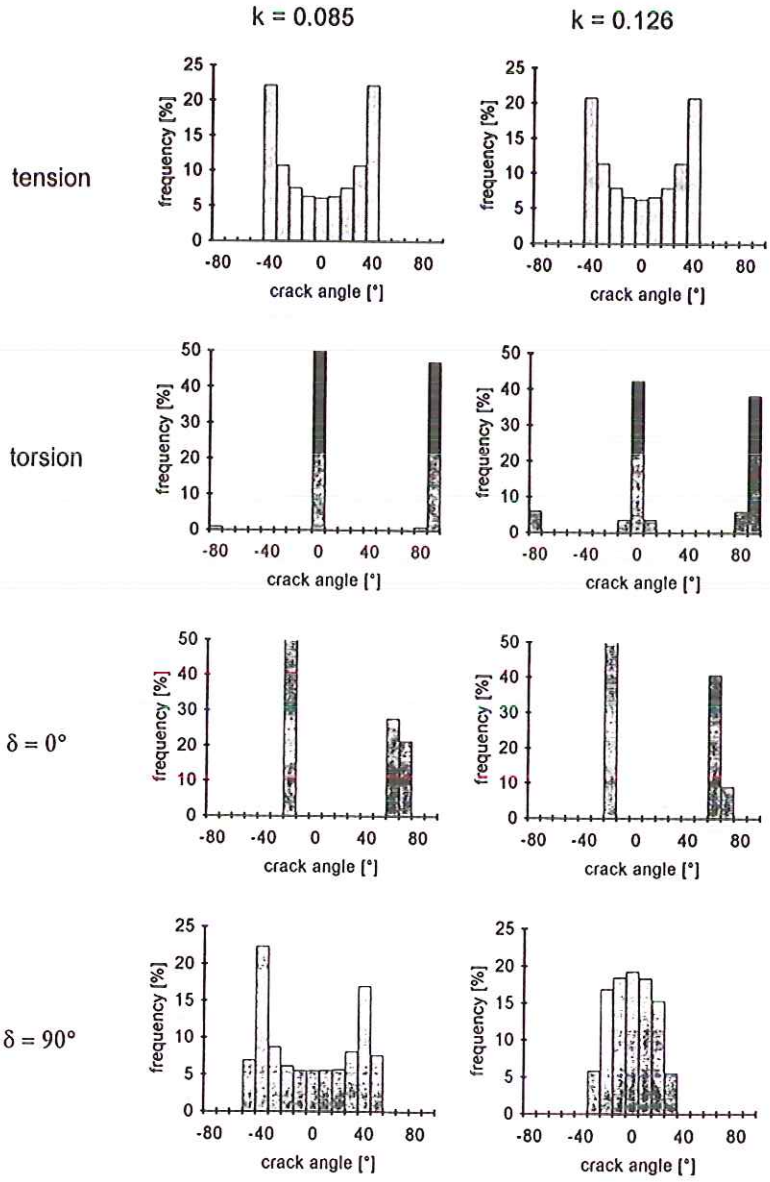

Fig 11 Frequencies of planes loaded with 95% of the maximum value of the Findley equivalent stress.

be equal to 0.169 for the ferritic steel and 0.252 for the austenitic steel, respectively. The histograms give a quite good description of the crack angle frequencies which were determined.

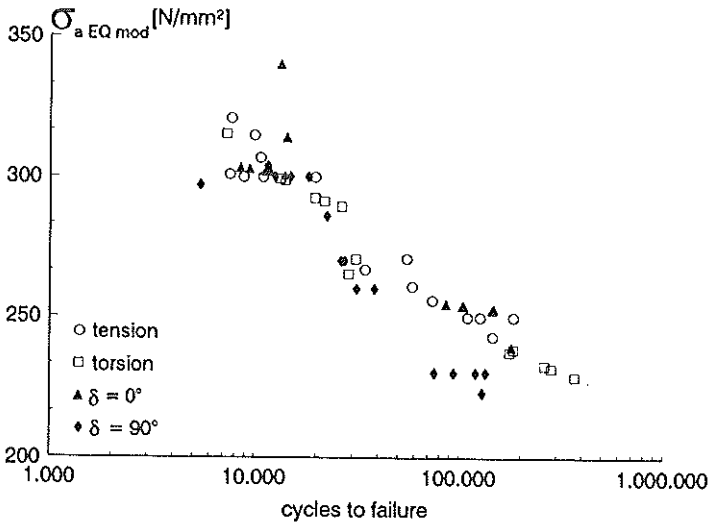

Fig 12 S–N curve of ferritic steel for different loadings.

6 Lifetime

In order to compare different loading conditions, the loading amplitudes were

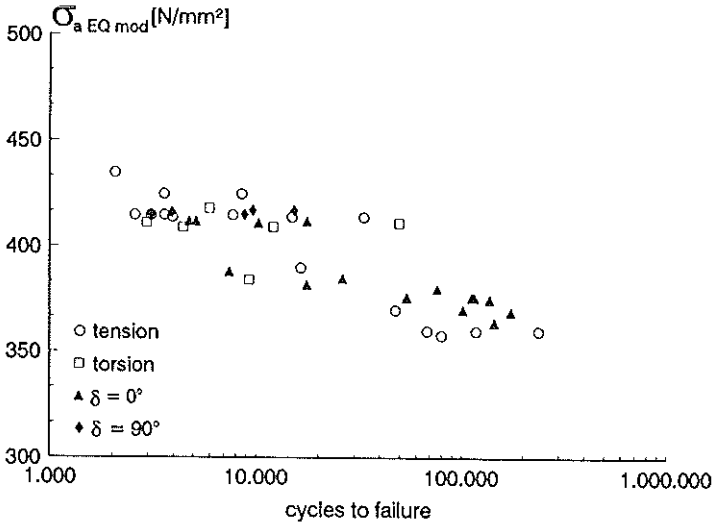

Fig 13 S–N curve of austenitic stainless steel for different loadings.

varied in order to explore different lifetimes. In Table 3 these loading amplitudes and the equivalent stresses for lifetimes $N_f = 10^4$ and $N_f = 10^5$ are collected. Comparing the different equivalent stress criteria the best fit of the results is given by the modification $\sigma_{a\,EQ}$ of the Tresca or von Mises criterion, respectively. Using this criterion the S-N diagrams of the two materials are plotted in Figs 12 and 13. There is only a slight deviation of the ferritic steel specimens for the out-of-phase loading at low amplitudes, where the lifetime is overestimated.

Table 3 Comparison of the equivalent stresses at different lifetimes for both materials

Ferritic steel $N_f \approx 10\,000$

	Loading parameters			*Equivalent stresses*			
	σ_a (N/mm²)	τ_a (N/mm²)	δ (deg)	$\sigma_{a\,EQ\,v.M.}$ (N/mm²)	$\sigma_{a\,EQ\,T}$ (N/mm²)	$\sigma_{a\,EQ\,F}$ k = 0.169 (N/mm²)	$\sigma_{a\,EQ\,mod}$ (N/mm²)
1	300	0	—	300	300	300	300
2	0	175	—	302	350	300	300
3	230	115	0	304	419	312	303
4	300	150	90	300	300	300	300

Ferritic steel $N_f \approx 100\,000$

	Loading parameters			*Equivalent stresses*			
	σ_a (N/mm²)	τ_a (N/mm²)	δ (deg)	$\sigma_{a\,EQ\,v.M.}$ (N/mm²)	$\sigma_{a\,EQ\,T}$ (N/mm²)	$\sigma_{a\,EQ\,F}$ k = 0.248 (N/mm²)	$\sigma_{a\,EQ\,mod}$ (N/mm²)
1	250	0	—	250	250	250	250
2	0	155	—	267	310	250	250
3	200	100	0	264	283	267	257
4	230	115	90	230	230	230	230

Austenitic stainless steel; high loading amplitude $N_f \approx 10\,000$

	Loading parameters			*Equivalent stresses*			
	σ_a (N/mm²)	τ_a (N/mm²)	δ (deg)	$\sigma_{a\,EQ\,v.M.}$ (N/mm²)	$\sigma_{a\,EQ\,T}$ (N/mm²)	$\sigma_{a\,EQ\,F}$ k = 0.252 (N/mm²)	$\sigma_{a\,EQ\,mod}$ (N/mm²)
1	410	0	—	410	410	410	410
2	0	255	—	440	510	410	410
3	320	160	0	423	453	426	411
4	410	205	90	410	410	410	410

7 Discussion

Microcracks initiate in slip planes subjected to maximum shear stress amplitude. Comparing the crack densities in Figs 6 and 7 with the maximum shear stress amplitude $\sigma_{a\,EQ\,T}$ shows an increasing crack initiation rate with increasing shear stress amplitude. For the ferritic steel at high loading amplitudes a saturation of the crack density is achieved.

Crack growth is determined by the shear stress amplitude, too, but will be also influenced by microstructural barriers and crack surface roughness. The bypassing of these obstacles will be supported by a normal stress perpendicular to the crack plane. Due to this, the cracks in planes loaded with high shear stress amplitude and an additional normal stress, as described by the Findley criterion, have an enhanced crack growth rate. This can be seen by comparing the measured crack angle frequencies with those calculated using a critical plane approach similar to the Findley criterion.

We conclude, that passing a barrier is easier in the ferritic steel than in the austenitic steel, which is documented by the difference in the value k of the Findley criterion. Additionally, we suppose that for a given shear stress amplitude, in the critical plane, passing a barrier is more difficult under torsion and in-phase loading, than under tension and out-of-phase loading. We find two reasons for this behaviour. First, under torsion and in-phase loading, the number of favourable crack growth planes is smaller than under out-of-phase and tension loading. The second reason is the stress normal to the crack growth plane. At a certain lifetime the maximum shear stress amplitude $\sigma_{a\,EQ\,T}$, and therefore the crack density, is smaller for tension loading than for torsion loading. Because of the normal stress amplitude on the plane of maximum shear stress amplitude being as high as the shear stress amplitude for tension loading – 0.7 times as high for the proportional loading and zero for torsion loading – the damaging effect of the different shear stress amplitudes is similar.

We conclude that cracks can pass a barrier more easily under tension or out-of-phase loading, than under torsion or in-phase loading. Therefore, we expect that the crack density at the occurrence of a macroscopic crack is higher for torsion and in-phase loading as observed for the austenitic steel and for the ferritic steel at low stress amplitudes. In the low-cycle fatigue area the crack density is very high. Therefore, barriers can easily be passed by crack linking under all loading conditions. Due to this, the torsion loading becomes more harmful for this loading amplitude. This is documented by the ratio of comparable damaging torsion to tension amplitude, which is equal to 0.58 in the low-cycle fatigue area and 0.66 for high-cycle fatigue.

Comparing the crack orientation under out-of-phase loading, we can state that for the ferritic steel under high-stress amplitudes, again due to the high crack density, barriers are easily passed by crack linking. Therefore the cracks initiated in any plane loaded with the maximum shear stress amplitude are able to grow. For the austenitic stainless steel the barriers are difficult to pass, because of the low crack density. Now the cracks initiated in planes additionally loaded by a high normal stress are more favoured to pass a barrier. The cracks counted in this investigation are longer than the medium grain size. All the cracks which are examined have already passed one or two grain boundaries. Due to this, cracks initiated in planes with a small normal stress will be stopped before being counted. This crack selection results in the observed crack orientation. The differences in the crack growth behaviour also influence the equivalent stress

criterion to be used. If the crack density did not allow to pass the barriers by crack linking, the torsional loading becomes less harmful, because there is no normal stress perpendicular to the plane of maximum shear stress. This is described by the modification of the Tresca criterion.

8 Conclusions

The deformation behaviour of the examined steels can be explained by the dislocation structure observed after loading. The ferritic steel produced a dislocation cell structure with a finer cell size after out-of-phase loading. This results in an additional mechanical hardening associated with out-of-phase loading. The austenitic steel shows a softening behaviour due to mechanical twinning. Therefore only a minimum of dislocation movement and dislocation interaction happens during loading, and no out-of-phase hardening effect is observed.

Microcracks are initiated on planes which are loaded with the maximum shear stress amplitude. Due to this, the crack density is determined by the Tresca equivalent stress. Crack growth is controlled by microstructural barriers and crack surface roughness. Passing these obstacles is more easy, if there is an additional normal stress on the crack plane.

For a certain lifetime this causes a higher tolerable Tresca equivalent stress for torsion and in-phase loading than for out-of-phase and tension loading. Additionally, the crack angle frequencies are influenced by the stress normal to the shear stress amplitude as described by the Findley criterion.

Acknowledgements

The authors gratefully acknowledge the support of the German Research Community (DFG).

References

(1) SOCIE, D. (1993) Critical plane approaches for multiaxial fatigue damage assessment, *Advances in Multiaxial Fatigue* (Edited by J. McDowell and R. Ellis), Philadelphia.
(2) PILO, D. (1979) Zum Wechselverformungsverhalten normalisierter unlegierter Stähle mit Kohlenstoffgehalten von 0,01 bis 1,092 Gew.-%, Dr. Thesis, University Karlsruhe.
(3) CAILLETAUD, G., DOQUET, V. and PINEAU, A. (1991) Cyclic multiaxial behaviour of an austenitic stainless steel: microstructural observations and micromechanical modelling, *Fatigue under Biaxial and Multiaxial Loading* (Edited by K. Kußmaul, D. L. McDiarmid, D. F. Socie) (ESIS Pub. 10) Mechanical Engineering Publications, London, pp. 131–149.
(4) LÖWISCH, G., BOMAS, H. and MAYR, P. (1992) Mikrostrukturelle Mechanismen des Schadensablaufs bei mehrachsiger, phasenverscholben schwingender Beanspruchung, *Schädigungsfrüherkennung und Schadensablauf bei Metallischen Bauteilen*, DVM, Darmstadt.
(5) RADHAKRISHNAN, V. M. and MUTOH, Y. (1986) On fatigue crack growth in Stage 1, *The Behaviour of Short Fatigue Cracks* (edited by K. J. Miller and E. R. de los Rios) EGF Pub. 1, Mechanical Engineering Publications, London, pp. 87–99.
(6) MUNZ, D. (1985) Bruchmechanische Bewertung von Ermüdungsrissen, *Ermüdungsverhalten metallischer Werkstoffe* (edited by D. Munz) DVM, Oberursel, pp. 129–167.
(7) TAYLOR, D. A. (1985) *Compendium of Fatigue Thresholds and Growth Rates*, Chameleon Press, London.